On the Adsorption of Aspartate Derivatives to Calcite Surfaces in Aqueous Environment

Robert Stepić,[†,‡,§] Lara Jurković,[¥,§] Ksenia Klementyeva,[‡] Marko Ukrainczyk,[¥] Matija Gredičak,[¶] David M. Smith,[†,*] Damir Kralj,[¥,*] and Ana–Sunčana Smith[†,‡,*]

[†] Group for Computational Life Sciences, Division of Physical Chemistry, Ruđer Bošković Institute (RBI), Bijenička cesta 54, 10000 Zagreb, Croatia

[‡] PULS Group, Institute for Theoretical Physics and Interdisciplinary Center for Nanostructured Films, FAU Erlangen–Nürnberg, Cauerstrasse 3, 91058 Erlangen, Germany

[¥] Laboratory for Precipitation Processes, Division of Material Chemistry, RBI, Bijenička cesta 54, 10000 Zagreb, Croatia

[¶] Laboratory for Biomimetic Chemistry, Division of Organic Chemistry and Biochemistry, RBI, Bijenička cesta 54, 10000 Zagreb, Croatia

Supporting Information

ABSTRACT: In many living organisms, biomolecules interact favorably with various surfaces of calcium carbonate. In this work, we have considered the interactions of aspartate (Asp) derivatives, as models of complex biomolecules, with calcite. Using kinetic growth experiments, we have investigated the inhibition of calcite growth by Asp, Asp_2 and Asp_3.This entailed the determination of a step-pinning growth regime as well as the evaluation of the adsorption constants and binding free energies for the three species to calcite crystals. These latter values are compared to free energy profiles obtained from fully atomistic molecular dynamics simulations. When using a flat (104) calcite surface in the models, the measured trend of binding energies is poorly reproduced. However, a more realistic model comprised of a surface with an island containing edges and corners, yields binding energies that compare very well with experiments. Surprisingly, we find that most binding modes involve the positively charged, ammonium group. Moreover, while attachment of the negatively charged carboxylate groups is also frequently observed, it is always balanced by the aqueous solvation of an equal or greater number of carboxylates. These effects are observed on all calcite features including edges and corners, the latter being associated with dominant affinities to Asp derivatives. As these features are also precisely the active sites for crystal growth, the experimental and theoretical results point strongly to a growth inhibition mechanism whereby these sites become blocked, preventing further attachment of dissolved ions and halting further growth.

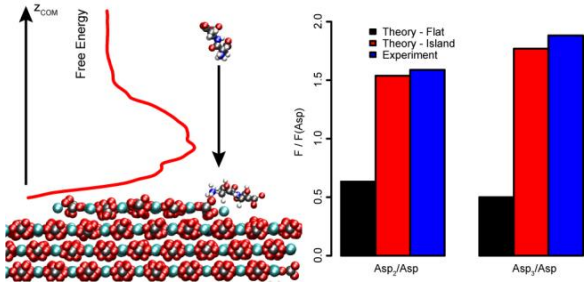

Minerals with exceptional mechanical properties are known to form when an inorganic crystal is grown in a medium that contains dissolved organic molecules. This process, known as biomineralization,[1] has garnered a lot of attention in recent years due to its relevance in functional material design.[2,4,5,6] The current hypothesis states that this phenomenon is predominantly driven by favorable electrostatic interactions between the inorganic ions forming the crystal lattice and biological matter in the form of negatively charged polyelectrolytes, mainly peptides, proteins, and polysaccharides.[3,5,7] Consequently, aspartic acid (Asp), which has a negatively charged side chain at biological pH, is found to be one of the most prominent constituents of bioactive peptides and proteins,[8] while the most studied minerals in this context are the naturally abundant carbonates,[9] and in particular, calcite.[10] Calcite grown in such an environment shows remarkable tensile strength and complete biocompatibility[11] making it a major candidate for many potential applications, the most prominent being in oil reservoirs,[12] CO_2 storage,[13] and especially drug delivery systems.[14,15,16,17,18] Despite this enormous potential, predictive understanding of the growth is still missing.

Inorganic calcite ($CaCO_3$) appears in various morphologies, of which the rhombohedrons bounded by the most stable calcite surfaces, the (104) faces, are the most frequent.[19] In contrast, many different shapes are exhibited in crystals grown in biological matrices as a result of the competition of constituent ions with organic molecules for the surface binding sites on the interfaces.[20,21] Consequently, the kinetic analyses of additive-inhibited crystal growth is one successful avenue of investigation, in particular, allowing the extraction of adsorption constants of a biomolecule to an inorganic surface, and allowing for the inference of the growth mode.[22,23] Specifically, if the additives bind strongly to active sites on the surfaces, they may block the sites and thus impair the crystal growth (step pinning).[24] Typically, this scenario is associated with a critical supersaturation of aqueous ions, at which growth can no longer occur ("dead zone"). An alternative scenario, known as kink blocking, is typical for impurities that adsorb weakly and briefly to the kinks at growing steps. As this situation leads only to an effective reduction in propagation and the kinetic growth coefficient, no dead zone

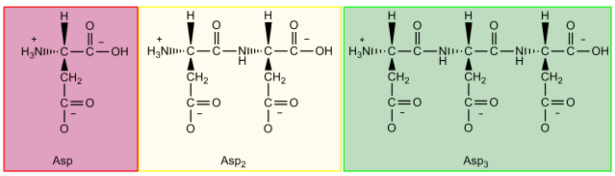

Scheme 1. Predominant chemical structures of Asp, Asp_2 and Asp_3 at nearly neutral pH.

should be observed.[25] If, on the other hand, the additives are incorporated into the growing crystal to a significant extent, they may distort it and increase the internal free energy.[26] This can lead to a lower effective supersaturation and a lower growth rate at a given concentration of constituent ions.[27]

The free energy of binding is also accessible by molecular dynamics (MD) simulations,[28,29,30,31] which, in addition, provide full atomic detail of the systems. However, because of the large number of available approaches and the sparsity of calibration against experiments,[30,32] an obvious general methodology for modelling interactions on an arbitrary calcite interface is subject to several important challenges.[33,34,35]

The first challenge is to model the interactions between the solid and the liquid phase.[28,29,31] Motivated by the method proposed for zeolites,[36] an attractive approach based on the AMBER[37] force field was recently developed.[38] However, the thereby-used[39] and other[40,41,30,42] models for the calcite are likely to be inferior for aqueous applications than a newer parametrization, which more accurately captures the thermodynamic properties of the water-calcite interface.[41] Nevertheless, the combination of the most promising models for the organic[38] and inorganic[41] phases has not yet been tested. The second challenge is the geometry of the calcite. Even though the (104) surface is the most abundant in the equilibrium, a realistic crystal model should account for different defects. Besides affecting the local water structure,[43-44] these features have different affinities for the organic additive, as shown recently for aspartic acid that demonstrated a preference to bind to acute edges and calcium corners.[45] These latest results, however, were not calibrated against experiment, which is the third challenge in the simulation field. With reported binding energies of Asp to various calcite surfaces ranging from[30] -2 kJ mol^{-1} to[46] -400 kJ mol^{-1}, and with the reliabilities only addressed for the interactions of selected monomeric species with calcite,[30,32] this aspect is of paramount importance. In particular, the significantly more complex challenge involving calibrated modeling of the binding of a polymeric series to calcite, has not yet been attempted.

In this work, we overcome these simulation challenges and determine the free energies of binding of an array of aspartate-based derivatives (Scheme 1), using a more realistic calcite surface, and advanced sampling techniques. By performing kinetic growth experiments, we are able to determine the growth regimes and generate benchmark values for the free energies of binding. Comparison of the modelling results with this data allows us to offer, with a high level of confidence, a systematic overview of the binding preferences of these biologically active building blocks to a complex calcite interface

Experimental Growth Inhibition. Analytical grade L-Asp and (L-Asp)$_2$ were used while the (L -Asp)$_3$ peptide was synthesized automatically from C- to N-terminus by the solid-phase Fmoc method (see supporting information: Section S1). Calcite seeds were prepared by the semi-continuous carbonation method (see Section S2).[47] The initial solution for crystal growth was composed of a mixture of calcium and carbonate ions, an Asp derivative and the calcite crystal seed. The growth experiments were performed in a thermostated double-walled glass vessel (see Section S3). The resulting change in pH, measured with a combined glass-calomel electrode, is induced by the incorporation of dissolved constituent ions (calcium and carbonate) into the crystal lattice, which caused changes in ionic equilibrium of carbonate ions to the growing crystal. Typical progress curves of calcite growth, pH versus time, obtained in the control system (black line), as well as in the systems containing different concentrations of Asp$_3$ are shown in Figure 1. It is evident that the calcite growth, indicated as a pH drop, started immediately after the addition of the seed in the systems (t=0). Relative to the control system, the crystal growth in the biomolecule-containing systems is progressively impeded by the increase in concentration of Asp$_3$. This is seen as the lowering of the slope of the

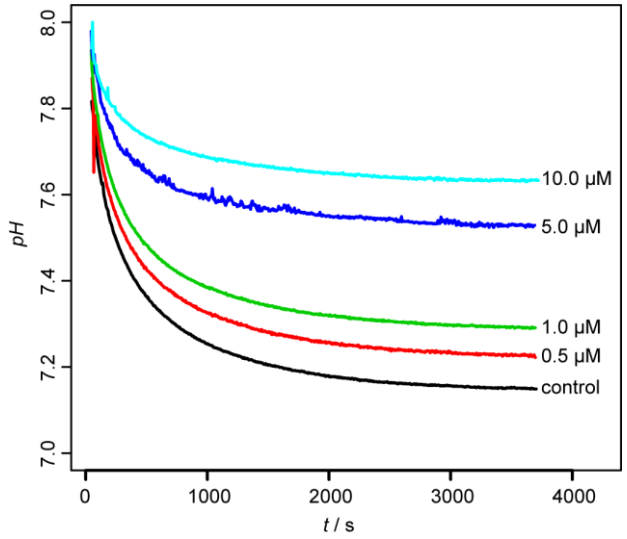

Figure 1. Progress curves, pH versus time, of the calcite growth in the precipitation systems (c($CaCl_2$)= c($NaHCO_3$)=5.0 mmol dm^{-3}; $pH_i \approx 8.0$; S-1 ≈ 2.5), containing systematically increasing concentrations of Asp$_3$. Model system (no biomolecules), is also indicated (bold black line). Highest concentration of the biomolecular additive resulted in the strongest reduction of growth of the calcite crystal.

respective curves. In addition, the growth in the presence of biomolecular additives apparently terminates at a specific pH (dead zone), which is higher for higher concentrations of the additive. This confirms that the added biomolecule binds relatively strongly to the available binding sites, impeding incorporation of calcium and carbonate ions and fully halting any further growth (step pinning). Additional data for the pH variation with different amounts of other additives (Asp and Asp$_2$), where we can observe a similar effect on growth, is given in Figure S1.

The solution composition at any moment of the process was calculated by using the measured pH and the known initial total concentrations of the reactants (Section S3). The detailed calculation procedure, which takes into account the respective protolytic equilibria and equilibrium constants, as well as the charge and mass balance equations, is described in previous work.[17,18] The crystal growth rate, R, was then calculated by numerical differentiation of the dissolved calcium concentration with respect to time and normalizing the result by the total surface area. The total surface area of the calcite seed was estimated by the multiple Brunauer-Emmet-Teller method,[48] and the increase of the area during growth was taken into account and calculated from the total calcium carbonate precipitate data. In terms of the supersaturation, the rate law can be described as $R = k_s(S - 1)\cdot \ln S$ (see Figure S2), as could be expected for the low-supersaturated systems.[27]

The mode and extent of the interactions of the biomolecules with the crystal surface can be quantitatively estimated by the means of Kubota and Mullin's mathematical model.[23] This approach uses the inhibited growth rate R relative to the growth rate in the absence of any additives, R_0, as the response variable and correlates it with the biomolecular coverage of the face active sites θ_{eq}, and their effectiveness α:

$$R/R_0 = 1 - \alpha\, \theta_{eq} \qquad (1)$$

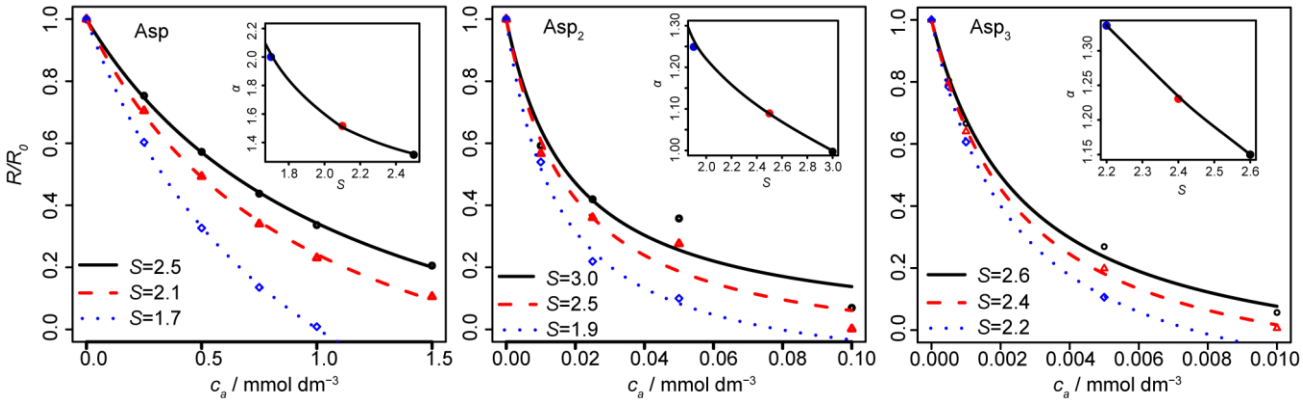

Figure 2. Relative growth rate reduction of calcite seed as a function of the concentration of different biomolecules, at different supersaturations, S. Lines are fitted isotherms in a two parametric non-linear fit where the biomolecule effectivness in blocking the growth α, and the adsorption constant K_{ad}, were varied. Insets: The dependancies of α on supersaturation. The line is guidance for the eye.

In this model, the effectiveness factor is assumed to be a stereochemical contribution of the respective dissolved organic molecules to the growth reduction. It is tied to the size, shape or orientation of the interacting biomolecules with respect to the active surface sites.[23]

In order to relate the concentration of the organic molecules in solution (c_a) and the growth rate reduction, the Langmuir adsorption model and isotherm are applied:

$$R/R_0 = 1 - \alpha[K_{ad}\, c_a/(1 + K_{ad}\, c_a)] \qquad (2)$$

In this expression, K_{ad} is the Langmuir adsorption constant for the process of biomolecule binding to the calcite surface, R is the growth rate in the system with some concentration of biomolecules and R_0 is the growth rate in the control system at a specific supersaturation. When $\alpha > 1$, the growth rate approaches zero even at incomplete surface coverage, while at $\alpha < 1$ the growth is not completely reduced, even at complete coverage of active sites for adsorption.

Figure 2 shows typical plots of the relative growth rate reduction (R/R_0) for calcite seeds at different relative supersaturations as a function of different concentrations (c_a) of Asp, Asp_2 and Asp_3, for selected supersaturations. The lines drawn through the experimental points are obtained by fitting the respective set of data with the function given by Eq. 2. We used a non-linear fitting procedure where two parameters were allowed to vary (K_{ad} and α), and the concentration of the additive was used as the independent variable. Values of the adsorption constants do not depend on the supersaturation. Thus, we have three independent measurements for each biomolecule. By taking the average over three independent fits, we obtained the following values of adsorption constants: K_{ad} = 1.0 ± 0.1 dm^3 mmol^{-1} (Asp); K_{ad} = 58.5 ± 8.5 dm^3 mmol^{-1} (Asp_2); K_{ad} = 397.2 ± 19.7 dm^3 mmol^{-1} (Asp_3). These values can be converted into the associated Gibbs free energies of binding -17.1 ± 0.2 kJ mol^{-1} (Asp), -27.2 ± 0.3 kJ mol^{-1} (Asp_2), -32.0 ± 0.1 kJ mol^{-1} (Asp_3), as shown in Table 1. The energy of binding of aspartate compares well with the value of -21 kJ mol^{-1} obtained previously by the means of fitting Langmuir, Langmuir-Freundlich, and Flory-Huggins isotherms to the fractional growth inhibition.[22]

Table 1. Binding energies of Asp-derivatives to calcite (units of kJ mol^{-1}) produced in this work.

	Experiment	Simulations (104)	Simulations (island)
Asp	-17.1 ± 0.2[(a)]	-30 ± 1[(b)]	-13 ± 1
Asp_2	-27.2 ± 0.3	-19 ± 1	-20 ± 1
Asp_3	-32.0 ±0.1	-15 ± 1	-23 ± 1

[(a)]Comparable to the value of 21 kJ mol^{-1} in Ref. 23 [(b)] Value of -46 kJ mol^{-1} is obtained using parametrization from Refs 30 and 36.

The experimental results we report here indicate that the energy of binding increases as we add more units of aspartate to the peptide. However, it does not do so linearly but rather in an asymptotic fashion. This also agrees with the hypothesis proposed in the literature.[22]

In addition to the adsorption constants, we determined the relationship between the biomolecular effectiveness factor α, and the supersaturation (Figure 2, insets). In all cases, we obtain $1 < \alpha < 3$, which is consistent with the step-pinning mechanism. We also observe that α is the highest for Asp, followed by Asp_3, whereas Asp_2 is the least effective of the three at comparable supersaturation values. Additional data for α, over a wider range of supersaturations, is presented in Figure S3.

Theoretical Binding Energies. We begin by considering the binding of the Asp-derivatives (Asp, Asp_2, Asp_3) to a flat (104) surface, (Section S5) primarily using the GROMACS 4.5.5 simulation package[49] (see Section S6 for other software employed). After an equilibration protocol, we performed umbrella-sampling simulations (147 ns/peptide, see Section S7) to calculate the potential of mean force (PMF). The combination of the multiple umbrella sampling runs is performed by weighted histogram analysis method (WHAM).[50] As a reaction coordinate, we use the vertical distance of the center of mass of the Asp-derivative from the first layer of the calcite crystal (z_{COM}). The position of the first layer is defined as the average position of interfacial calcium ions.

Parameters for the zwitterionic Asp-derivatives are extracted from the AMBER force field[51,52] and combined with TIP3P water.[53] Given that the thermodynamics of the interfacial water is an important determinant of the derivative binding to calcite, the crystal is modeled using the force field of Raiteri et al.[41] The classic combination rules for organic-inorganic interactions are avoided as much as possible, because of the significant disparity in the charge magnitudes in the two subsystems, following the recommendation of Freeman et al.[38] Accordingly, the cross-terms involving calcium

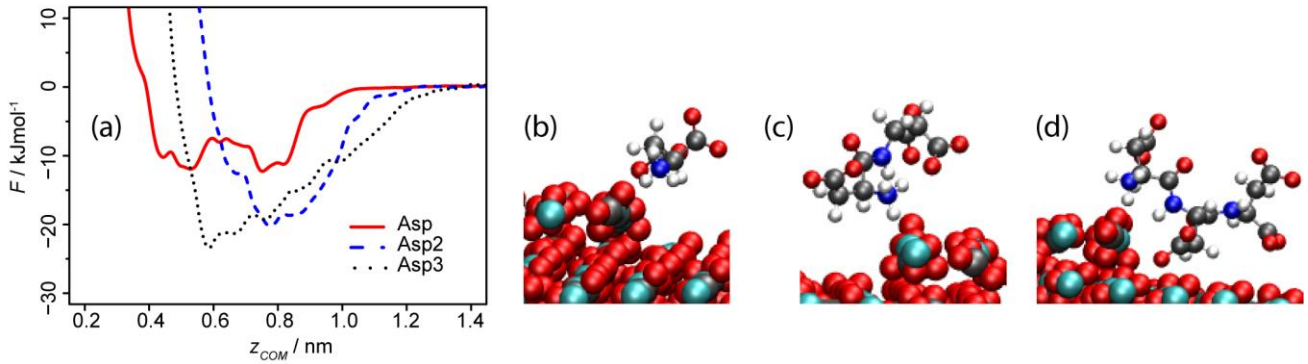

Figure 3. Interactions of Asp derivatives with the calcite surface containing an island (a) Potentials of mean force for binding of Asp, Asp_2 and Asp_3. Structures representing common binding modes for (b) Asp, (c) Asp_2, and (d) Asp_3.

are obtained using the Schroeder[36] method, the interactions with the oxygen were evaluated using Lorentz-Berthelot combination rules, while the interactions with carbon were taken from the AMBER[37] force field (further details on the force field are given in Section S8). In combination with a simple model for calcite,[39] this approach yielded very accurate results for different organic functional groups, when compared to the ab initio data.[38]

Combining these cross-terms with the Raiteri calcite force field, and calculating the PMF for Asp binding to the neutral (104) surface (Figure S6) provides a very high binding energy (-46 kJ mol^{-1}), well outside of the experimental range. After a careful analysis, we find the source of this over-binding in the dispersion interactions of crystal oxygen with aspartate atoms, which are therefore replaced by the AMBER force field[51,41] parameters, effectively eliminating the need to use any combination rules for inorganic-organic cross terms (see Tables S1-S3). The calculation of the PMF (Figure S6) with this modification yields a 16 kJ mol^{-1} reduction of the binding free energy, which now adopts a value of -30 kJ mol^{-1}, significantly closer to the experimental measurements. At the same time, the crystal-water interface remains intact, consistent with the thermodynamics of solvation of calcium and carbonate ions.

We repeat the analogous simulation procedure and constructed two additional free energy profiles for the binding of Asp_2 and Asp_3 to the (104) surface of calcite (Figure S7). As shown in Table 1, the free energy of binding of Asp_2 amounts to -19 kJ mol^{-1} and for Asp_3 it is -15 kJ mol^{-1}. Not only do the individual binding energies deviate from the experiment, but also the experimental trend within the series is not recovered. This indicates an issue beyond the level of the force field. For this reason, we introduce a calcite surface with an island possessing six distinct features (see Section S5):[34] acute (AE) and obtuse (OE) edges, acute (ACC) and obtuse carbonate (OCC) corners, a calcium corner (CaC), and a central surface exposing a (104) plane (MI).

To evaluate the binding of Asp, Asp_2, and Asp_3 to such a complex surface, we first equilibrate each Asp-derivative on each of the six features and produce six 147 ns sampling runs (total of 882 ns/Asp-derivative), which are consequently combined using WHAM. The corresponding average profiles for Asp, Asp_2 and Asp_3 (Figure 3) provide the free energies of binding of -13 kJ mol^{-1}, -20 kJ mol^{-1} and -23 kJ mol^{-1}, respectively (Table 1). Despite being slightly, yet systematically too low, these binding energies are in an excellent agreement with experimental data, especially for such a challenging series.

Analysis of dominant interactions. With the reliability of the computational model established, we turn to investigating the binding modes of the Asp-derivatives to the calcite surfaces.

We first assess the frequency of the interactions with the various island features, using a self-developed analysis tool (Section S10). This results in a set of normalized histograms (Figure 4), which

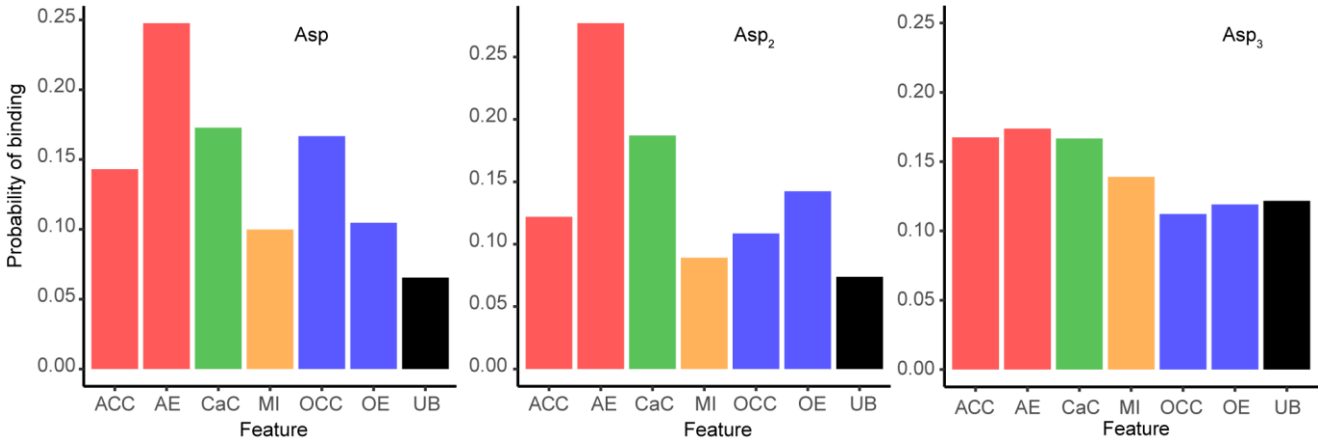

Figure 4. Probability of a biomolecule (Asp, Asp_2, Asp_3) to be bound to a certain feature of the island: acute carbonate corner (ACC), acute edge (AE), calcium corner (CaC), central surface exposing a (104) plane (MI), obtuse carbonate corner (OCC), obtuse edge (OE), or unbound (UB).

show that Asp and Asp_2 have a preference for binding to the acute edge and the calcium corners, similar to that reported for Asp previously.[45] This preference seems to diminish for Asp_3, which is in line with investigations of the inhibited growth of a series of Asp derivatives with Atomic Force Microscopy.[46] Further inspection of Figure 4 shows that all of the Asp-derivatives, however, tend to be drawn from the middle to the edges and corners of the island. Given that these features are precisely the active sites during crystal growth; this finding explains the inhibition of growth upon the addition of Asp-derivatives (Figure 1 and S1). Furthermore, the relatively large binding affinities are in agreement with the appearance of the experimentally obtained dead zone and the complete blocking of the growth at sufficient additive concentration.

The overall binding free energies (and the associated binding modes) are, however, the result of interactions between not only the additive and the features of surface but they also contain large contributions from the (de)solvation of the Asp derivatives and the ions on the calcite surface, in a unique way over each feature of the surface. However, several common aspects, which seem to dominate the interactions of the Asp derivatives, can be extracted. For example, the Asp monomer, in its lowest-energy minimum on the island (Figure 3) and for the most prominent bonding modes identified for each of the six surface features (Figure S9, Table S4), displays a persistent interaction between the positively charged ammonium group and the solid phase. The majority of these modes also exhibit binding through the C-terminal carboxylate, whereas the sidechain carboxylate remains solvated in all cases. Interestingly, analogous features are associated with the dominant minimum for Asp on the pure (104) surface (Figure S6).

For Asp_2 on the island (Figures 3 and S10), the situation is very similar to that for Asp. Specifically, the ammonium group establishes a persistent (yet slightly more distant, Table S5) contact with the calcite, whereas at most one of three carboxylate groups is also bound to the surface. This leaves at least two carboxylate groups in solution, explaining the larger values of z_{COM} associated with the minimum in the overall PMF (Figure 3). On the flat (104) surface both Asp_2, but also Asp_3 show the ammonium group always bound to the surface together with at most one carboxylate group also bound (Figure S8). The remaining carboxylate groups continue to exhibit a strong preference for being solvated. This preference appears to be responsible for the positions of the minima being shifted to higher values of z_{COM} and, indeed, the decreasing binding energies as the number of Asp units is increased (Table 1).

Like Asp_2, Asp_3 on the island (Figures 3 and S11) also exhibits a dominance of ammonium-mediated binding (including close contacts, Table S6). However, in this case, at most two carboxylates are found in direct simultaneous contact with the calcite, while at least two appear in the aqueous medium. More often than not, the bound carboxylates originate from one of the side chains so that, on average, the COM of Asp_3 is closer to the surface than that of Asp_2. Precisely this feature should be seen in the context of the efficiency for the growth inhibition of Asp_3, relative to Asp_2 (larger values of α for comparable supersaturation), which is obviously a stereochemical contribution,[23] not just a consequence of binding affinity. This effect is likely to be associated with the fact that Asp_3 (as well as Asp) can access the crystal edges more closely than Asp_2, as discussed above, and is thus able to inhibit the crystal growth more effectively. Importantly, such a conclusion is only extractable from the island model, as the derivative accessibility to the flat (104) surface offer the opposite trend.

Summary. The primary focus of our work was to explore the binding of Asp, Asp_2 and Asp_3 to calcite using a combined experimental and theoretical approach. The experiments clearly revealed that the additives exhibited an inhibitory effect on crystal growth, which increased asymptotically with the length of the peptide chain. The observation of a dead zone in the growth kinetics and the evaluation of the effectiveness factors confirmed a strong binding of the additives to the face active sites and the presence of a step-pinning mechanism of growth inhibition. This is supported by the quantitative analysis of the inhibition kinetics, which allows us to provide reliable estimates of the relatively large free energies of binding of the Asp, Asp_2 and Asp_3 to the growing crystal seed.

With the experimental data in hand, we were able to show that a basic force field approach results in significant over-binding of Asp to the flat calcite (104) surface. While this shortcoming was somewhat rectified by modifying certain inorganic-organic cross terms, the energetic effect of increasing the Asp content on the flat surface was completely opposite to that observed in experiment. Using a more elaborate surface model, however, resulted in a series of binding free energies with good qualitative and quantitative agreement with the experimental measurements. This result lends significant credibility to the underlying theoretical model and allows the investigation of binding properties with confidence.

Our results demonstrate, perhaps counterintuitively, that the most persistent binding feature of the Asp derivatives to calcite is the attachment of the positively charged ammonium group. This is frequently accompanied by simultaneous carboxylate attachment but always balanced by the solvation of one or more carboxylates in the aqueous phase. We presume that this balance is the primary factor responsible for the asymptotic growth of the binding energies as the number of Asp units is increased, a result also previously obtained in the context of inhibited growth[22] (see Figure S12).

A probabilistic analysis shows that, for all three Asp derivatives, the additive prefers interactions with the edges and corners of the island than with the (104) surfaces in the center of the island or the bulk of the crystal. While many different structural motifs can be identified and classified, the overall indication is that the edges and corners are the preferred location for additive absorption. This, in turn, confirms that the growth inhibition mechanism relies primarily on the blocking of these sites, preventing further incorporation of dissolved ions and, hence, crystal growth.

ASSOCIATED CONTENT

Supporting Information

Sections S1-S11, Figures S1-S12, Tables S1-S6 (details on peptide synthesis, calcite seed preparation, growth kinetics, inhibition factor, simulation system, software, sampling protocols, force field, geometry of the binding modes and biding trends). The Supporting Information material is available free of charge on the ACS Publications website at http://pubs.acs.org.

AUTHOR INFORMATION

Corresponding Author

*E–mail: ana-suncana.smith@fau.de
*E–mail: Damir.Kralj@irb.hr
*E–mail: David.Smith@irb.hr

Author Contributions

§These authors contributed equally.

ACKNOWLEDGMENT

The Croatian Science Foundation is gratefully acknowledged for the financial support (project numbers: IP-11–2013–8238 (DS) and IP-11-2013-5055 (DK)). We also thank the Cluster of Excellence Engineering of Advanced Materials (EAM) and the Regionale RechenZentrum Erlangen (RRZE) Friedrich–Alexander–Universität Erlangen–Nürnberg (FAU) for the computational resources. We thank Zlatko Brkljača (RBI) for assistance with construction of the calcite surfaces and Ivanka Jerić for helpful discussions in the early

stages of the project. We thank Radha D. Banhati for careful reading of the manuscript.

REFERENCES

1. Estroff, L. A. Introduction: Biomineralization. *Chem. Rev.* **2008,** *108*, 4329-4331.
2. DeOliveira, D. B.; Laursen, R. A. Control of Calcite Crystal Morphology by a Peptide Designed To Bind to a Specific Surface. *J. Am. Chem. Soc.* **1997,** *119*, 10627-10631.
3. Dickerson, M. B.; Sandhage, K. H.; Naik, R. R. Protein- and peptide-directed syntheses of inorganic materials. *Chem. Rev.* **2008,** *108*, 4935-4978.
4. Shen, J.-W.; Li, C.; van der Vegt, N. F. A.; Peter, C. Understanding the Control of Mineralization by Polyelectrolyte Additives: Simulation of Preferential Binding to Calcite Surfaces. *J. Phys. Chem. C* **2013,** *117*, 6904-6913.
5. Sand, K. K.; Pedersen, C. S.; Sjöberg, S.; Nielsen, J. W.; Makovicky, E.; Stipp, S. L. S. Biomineralization: Long-Term Effectiveness of Polysaccharides on the Growth and Dissolution of Calcite. *Cryst. Growth Des.* **2014,** *14*, 5486-5494.
6. So, C. R.; Liu, J.; Fears, K. P.; Leary, D. H.; Golden, J. P.; Wahl, K. J. Self-Assembly of Protein Nanofibrils Orchestrates Calcite Step Movement through Selective Nonchiral Interactions. *ACS Nano* **2015,** *9*, 5782-5791.
7. Pai, R. K.; Pillai, S. Divalent cation-induced variations in polyelectrolyte conformation and controlling calcite morphologies: direct observation of the phase transition by atomic force microscopy. *J. Am. Chem. Soc.* **2008,** *130*, 13074-13078.
8. Addadi, L.; Weiner, S. Control and Design Principles in Biological Mineralization. *Angew. Chem. Int. Ed. Engl.* **1992,** *31*, 153-169.
9. Cusack, M.; Freer, A. Biomineralization: Elemental and Organic Influence in Carbonate Systems. *Chem. Rev.* **2008,** *108*, 4433-4454.
10. Espinosa, H. D.; Rim, J. E.; Barthelat, F.; Buehler, M. J. Merger of structure and material in nacre and bone – Perspectives on de novo biomimetic materials. *Prog. Mater Sci.* **2009,** *54*, 1059-1100.
11. Sommerdijk, N. A. J. M.; de With, G. Biomimetic $CaCO_3$ Mineralization using Designer Molecules and Interfaces. *Chem. Rev.* **2008,** *108*, 4499-4550.
12. Jensenius, J.; Burruss, R. C. Hydrocarbon-water interactions during brine migration: Evidence from hydrocarbon inclusions in calcite cements from Danish North Sea oil fields. *Geochim. Cosmochim. Acta* **1990,** *54*, 705-713.
13. Zhao, T.; Guo, B.; Zhang, F.; Sha, F.; Li, Q.; Zhang, J. Morphology Control in the Synthesis of $CaCO_3$ Microspheres with a Novel CO_2-Storage Material. *ACS Appl. Mater. Inter.* **2015,** *7*, 15918-15927.
14. Ueno, Y.; Futagawa, H.; Takagi, Y.; Ueno, A.; Mizushima, Y. Drug-incorporating calcium carbonate nanoparticles for a new delivery system. *J. Control. Release* **2005,** *103*, 93-98.
15. Zhang, J.; Li, Y.; Xie, H.; Su, B.-L.; Yao, B.; Yin, Y.; Li, S.; Chen, F.; Fu, Z. Calcium Carbonate Nanoplate Assemblies with Directed High-Energy Facets: Additive-Free Synthesis, High Drug Loading, and Sustainable Releasing. *ACS Appl. Mater. Inter.* **2015,** *7*, 15686-15691.
16. Ogomi, D.; Serizawa, T.; Akashi, M. Controlled release based on the dissolution of a calcium carbonate layer deposited on hydrogels. *J. Control. Release* **2005,** *103*, 315-323.
17. Ukrainczyk, M.; Grebičak, M.; Jerić, I.; Kralj, D. Interactions of salicylic acid derivatives with calcite crystals. *J. Colloid Interface Sci.* **2012,** *365*, 296-307.
18. Ukrainczyk, M.; Grebičak, M.; Jerić, I.; Kralj, D. Interactions of Scalenohedral Calcite Crystals with Acidic Amino Acid Derivatives of Salicylic Acid. *Cryst. Growth Des.* **2014,** *14*, 4335-4346.
19. Morse, J. W.; Arvidson, R. S.; Lüttge, A. Calcium Carbonate Formation and Dissolution. *Chem. Rev.* **2007,** *107*, 342-381.
20. Njegić-Džakula, B.; Falini, G.; Brečević, L.; Skoko, Ž.; Kralj, D. Effects of initial supersaturation on spontaneous precipitation of calcium carbonate in the presence of charged poly-l-amino acids. *J. Colloid Interface Sci.* **2010,** *343*, 553-563.
21. Buljan Meić, I.; Kontrec, J.; Domazet Jurašin, D.; Njegić Džakula, B.; Štajner, L.; Lyons, D. M.; Dutour Sikirić, M.; Kralj, D. Comparative Study of Calcium Carbonates and Calcium Phosphates Precipitation in Model Systems Mimicking the Inorganic Environment for Biomineralization. *Cryst. Growth Des.* **2017,** *17*, 1103-1117.
22. Montanari, G.; Lakshtanov, L. Z.; Tobler, D. J.; Dideriksen, K.; Dalby, K. N.; Bovet, N.; Stipp, S. L. S. Effect of Aspartic Acid and Glycine on Calcite Growth. *Cryst. Growth Des.* **2016,** *16*, 4813-4821.
23. Kubota, N.; Mullin, J. W. A kinetic model for crystal growth from aqueous solution in the presence of impurity. *J. Cryst. Growth* **1995,** *152*, 203-208.
24. Cabrera, N.; Vermilyea, D. A. The Growth of Crystal From Solution. Doremus, R. H.; Roberts, B. W.; Turnbull, D., Eds. Chapman & Hall: London, 1958; p p. 393.
25. Chernov, A. A. The Spiral Growth of Crystals. *Sov. Phys. Usp.* **1961,** *4*, 116-148.
26. van Enckevort, W. J. P.; van den Berg, A. C. J. F. Impurity blocking of crystal growth: a Monte Carlo study. *J. Cryst. Growth* **1998,** *183*, 441-455.
27. Davis, K. J.; Dove, P. M.; De Yoreo, J. J. The Role of Mg2+ as an Impurity in Calcite Growth. *Science* **2000,** *290*, 1134-1137.
28. Heinz, H.; Lin, T.-J.; Kishore Mishra, R.; Emami, F. S. Thermodynamically Consistent Force Fields for the Assembly of Inorganic, Organic, and Biological Nanostructures: The INTERFACE Force Field. *Langmuir* **2013,** *29*, 1754-1765.
29. Olsen, R.; Leirvik, K. N.; Kvamme, B.; Kuznetsova, T. Adsorption Properties of Triethylene Glycol on a Hydrated $\{10\bar{1}4\}$ Calcite Surface and Its Effect on Adsorbed Water. *Langmuir* **2015,** *31*, 8606-8617.
30. Raiteri, P.; Demichelis, R.; Gale, J. D.; Kellermeier, M.; Gebauer, D.; Quigley, D.; Wright, L. B.; Walsh, T. R. Exploring the influence of organic species on pre- and post-nucleation calcium carbonate. *Faraday Discuss.* **2012,** *159*, 61-85.
31. Ruiz-Agudo, E.; Di Tommaso, D.; Putnis, C. V.; de Leeuw, N. H.; Putnis, A. Interactions between Organophosphonate-Bearing Solutions and $(10\bar{1}4)$ Calcite Surfaces: An Atomic Force Microscopy and First-Principles Molecular Dynamics Study. *Cryst. Growth Des.* **2010,** *10*, 3022-3035.
32. Sparks, D. J.; Romero-González, M. E.; El-Taboni, E.; Freeman, C. L.; Hall, S. A.; Kakonyi, G.; Swanson, L.; Banwart, S. A.; Harding, J. H. Adsorption of poly acrylic acid onto the surface of calcite: an experimental and simulation study. *Phys. Chem. Chem. Phys.* **2015,** *17*, 27357-27365.
33. Harding, J. H.; Duffy, D. M. The challenge of biominerals to simulations. *J. Mater. Chem.* **2006,** *16*, 1105-1112.
34. Harding, J. H.; Duffy, D. M.; Sushko, M. L.; Rodger, P. M.; Quigley, D.; Elliott, J. A. Computational techniques at the organic-inorganic interface in biomineralization. *Chem. Rev.* **2008,** *108*, 4823-4854.
35. Demichelis, R.; Schuitemaker, A.; Garcia, N. A.; Koziara, K. B.; De La Pierre, M.; Raiteri, P.; Gale, J. D. Simulation of Crystallization of Biominerals. *Ann. Rev. Mater. Res.* **2018,** *48*, 327-352.
36. Schröder, K.-P.; Sauer, J.; Leslie, M.; Richard, C.; Catlow, A.; Thomas, J. M. Bridging hydrodyl groups in zeolitic catalysts: a computer simulation of their structure, vibrational properties and acidity in protonated faujasites (HxY zeolites). *Chem. Phys. Lett.* **1992,** *188*, 320-325.
37. Ponder, J. W.; Case, D. A. Force Fields for Protein Simulations. *Adv. Protein Chem.* **2003,** *66*, 27-85.
38. Freeman, C. L.; Harding, J. H.; Cooke, D. J.; Elliott, J. A.; Lardge, J. S.; Duffy, D. M. New forcefields for modeling biomineralization processes. *J. Phys. Chem. C* **2007,** *111*, 11943-11951.
39. Pavese, A.; Catti, M.; Price, G. D.; Jackson, R. A. Interatomic potentials for $CaCO_3$ polymorphs (calcite and aragonite), fitted to elastic and vibrational data. *Phys. Chem. Miner.* **1992,** *19*, 80-87.
40. Pavese, A.; Catti, M.; Parker, S. C.; Wall, A. Modelling of the thermal dependence of structural and elastic properties of calcite, $CaCO_3$. *Phys. Chem. Miner.* **1996,** *23*, 89-93.
41. Raiteri, P.; Gale, J. D.; Quigley, D.; Rodger, P. M. Derivation of an Accurate Force-Field for Simulating the Growth of Calcium Carbonate from Aqueous Solution: A New Model for the Calcite−Water Interface. *J. Phys. Chem. C* **2010,** *114*, 5997-6010.
42. Xiao, S.; Edwards, S. A.; Gräter, F. A New Transferable Forcefield for Simulating the Mechanics of $CaCO_3$ Crystals. *J. Phys. Chem. C* **2011,** *115*, 20067-20075.

43. Wolthers, M.; Di Tommaso, D.; Du, Z.; de Leeuw, N. H. Calcite surface structure and reactivity: molecular dynamics simulations and macroscopic surface modelling of the calcite-water interface. *Phys. Chem. Chem. Phys.* **2012,** *14*, 15145-15157.

44. De La Pierre, M.; Raiteri, P.; Gale, J. D. Structure and Dynamics of Water at Step Edges on the Calcite {10$\bar{1}$4} Surface. *Cryst. Growth Des.* **2016,** *16*, 5907-5914.

45. Nada, H. Difference in the Conformation and Dynamics of Aspartic Acid on the Flat Regions, Step Edges, and Kinks of a Calcite Surface: A Molecular Dynamics Study. *J. Phys. Chem. C* **2014,** *118*, 14335-14345.

46. Elhadj, S.; Salter, E. A.; Wierzbicki, A.; De Yoreo, J. J.; Han, N.; Dove, P. M. Peptide Controls on Calcite Mineralization: Polyaspartate Chain Length Affects Growth Kinetics and Acts as a Stereochemical Switch on Morphology. *Cryst. Growth Des.* **2005,** *6*, 197-201.

47. Ukrainczyk, M.; Kontrec, J.; Babić-Ivančić, V.; Brečević, L.; Kralj, D. Experimental design approach to calcium carbonate precipitation in a semicontinuous process. *Powder Technol.* **2007,** *171*, 192-199.

48. Brunauer, S.; Emmett, P. H.; Teller, E. Adsorption of Gases in Multimolecular Layers. *J. Am. Chem. Soc.* **1938,** *60*, 309-319.

49. Pronk, S.; Páll, S.; Schulz, R.; Larsson, P.; Bjelkmar, P.; Apostolov, R.; Shirts, M. R.; Smith, J. C.; Kasson, P. M.; van der Spoel, D.; Hess, B.; Lindahl, E. GROMACS 4.5: a high-throughput and highly parallel open source molecular simulation toolkit. *Bioinformatics* **2013,** *29*, 845-854.

50. Hub, J. S.; de Groot, B. L.; van der Spoel, D. g_wham—A Free Weighted Histogram Analysis Implementation Including Robust Error and Autocorrelation Estimates. *J. Chem. Theory Comput.* **2010,** *6*, 3713-3720.

51. Best, R. B.; Hummer, G. Optimized molecular dynamics force fields applied to the helix-coil transition of polypeptides. *J. Phys. Chem. B* **2009,** *113*, 9004-9015.

52. Lindorff-Larsen, K.; Piana, S.; Palmo, K.; Maragakis, P.; Klepeis, J. L.; Dror, R. O.; Shaw, D. E. Improved side-chain torsion potentials for the Amber ff99SB protein force field. *Proteins* **2010,** *78*, 1950-1958.

53. Jorgensen, W. L.; Chandrasekhar, J.; Madura, J. D.; Impey, R. W.; Klein, M. L. Comparison of simple potential functions for simulating liquid water. *J. Chem. Phys.* **1983,** *79*, 926-935.

TOC